

ATMOSPHERES AND SPECTRA OF STRONGLY MAGNETIZED NEUTRON STARS – III.
PARTIALLY IONIZED HYDROGEN MODELS

WYNN C. G. HO AND DONG LAI

Center for Radiophysics and Space Research, Department of Astronomy, Cornell University, Ithaca, NY 14853
wynnho, dong@astro.cornell.edu

ALEXANDER Y. POTEKHIN

Ioffe Physico-Technical Institute, Politekhnicheskaya 26, 194021, St. Petersburg, Russia;
Isaac Newton Institute of Chile, St. Petersburg Branch, Russia
palex@astro.ioffe.rssi.ru

AND

GILLES CHABRIER

CRAL (UMR CNRS No. 5574), Ecole Normale Supérieure de Lyon, 69364 Lyon Cedex 07, France
chabrier@ens-lyon.fr*Draft version November 7, 2018*

ABSTRACT

We construct partially ionized hydrogen atmosphere models for magnetized neutron stars in radiative equilibrium with surface fields $B = 10^{12} - 5 \times 10^{14}$ G and effective temperatures $T_{\text{eff}} \sim$ a few $\times 10^5 - 10^6$ K. These models are based on the latest equation of state and opacity results for magnetized, partially ionized hydrogen plasmas that take into account various magnetic and dense medium effects. The atmospheres directly determine the characteristics of thermal emission from isolated neutron stars. For the models with $B = 10^{12} - 10^{13}$ G, the spectral features due to neutral atoms lie at extreme UV and very soft X-ray energy bands and therefore are difficult to observe. However, the continuum flux is also different from the fully ionized case, especially at lower energies. For the superstrong field models ($B \gtrsim 10^{14}$ G), we show that the vacuum polarization effect not only suppresses the proton cyclotron line as shown previously, but also suppresses spectral features due to bound species; therefore spectral lines or features in thermal radiation are more difficult to observe when the neutron star magnetic field is $\gtrsim 10^{14}$ G.

Subject headings: magnetic fields – radiative transfer – stars: atmospheres – stars: magnetic fields – stars: neutron – X-rays: stars

1. INTRODUCTION

Thermal radiation from the surface of isolated neutron stars (NSs) can provide invaluable information on the physical properties and evolution of NSs. In the last few years, such radiation has been detected from radio pulsars (see Becker 2000; Pavlov, Zavlin, & Sanwal 2002), from old and young radio-quiet NSs (see Treves et al. 2000; Pavlov et al. 2002), and from soft gamma-ray repeaters (SGRs) and anomalous X-ray pulsars (AXPs) (see Hurley 2000; Mereghetti et al. 2002a), which form a potentially new class of NSs (“magnetars”) endowed with superstrong ($B \gtrsim 10^{14}$ G) magnetic fields (see Thompson & Duncan 1996; Thompson 2001). The NS surface emission is mediated by the thin atmospheric layer (with scale height $\sim 0.1 - 10$ cm and density $\sim 0.1 - 10^3$ g cm $^{-3}$) that covers the stellar surface. Therefore, to properly interpret the observations of NS surface emission and to provide accurate constraints on the physical properties of NSs, it is important to understand in detail the radiative properties of NS atmospheres in the presence of strong magnetic fields (see Pavlov et al. 1995; Ho & Lai 2001, 2003a; Zavlin & Pavlov 2002 for more detailed references on observations and on previous works of NS atmosphere modeling).

This paper is the third in a series where we systematically investigate the atmosphere and spectra of strongly magnetized NSs. In Ho & Lai (2001, hereafter HL01), we

constructed self-consistent NS atmosphere models in radiative equilibrium with magnetic field $B \sim 10^{12} - 10^{15}$ G and effective temperature $T_{\text{eff}} \sim 10^6 - 10^7$ K and assuming the atmosphere is composed of fully ionized hydrogen or helium; we focused on the effect of the ion cyclotron resonance at $E = E_{Bi} = 0.63 Y_e (B/10^{14}$ G) keV, where $Y_e = Z/A$ is the electron fraction and Z and A are the atomic charge and atomic mass of the ion, respectively, and showed that the spectra can exhibit a broad feature due to the ion resonance (see also Zane et al. 2001). In Ho & Lai (2003a, hereafter HL03; see also Lai & Ho 2002, 2003), we studied the effect of vacuum polarization on the atmosphere structure and radiation spectra of strongly magnetized NSs. Polarization of the vacuum due to virtual e^+e^- pairs becomes significant when $B \gtrsim B_Q$, where $B_Q = m_e^2 c^3 / e\hbar = 4.414 \times 10^{13}$ G is the critical QED magnetic field strength. Vacuum polarization modifies the dielectric property of the medium and the polarization of photon modes (e.g., Adler 1971; Tsai & Erber 1975; Gnedin, Pavlov, & Shibanov 1978; Heyl & Hernquist 1997), thereby altering the radiative scattering and absorption opacities (e.g., Mészáros & Ventura 1979; Pavlov & Gnedin 1984; see Mészáros 1992 for review). We showed that vacuum polarization leads to a broad depression in the high-energy ($E \gtrsim$ a few keV) radiation flux from the atmospheres and hence softer high energy

tails, as compared to models without vacuum polarization. The depression in the spectrum is broad because of the large density gradient in the atmosphere. This depression of continuum flux also strongly suppresses the equivalent width of the ion cyclotron line and makes the line more difficult to observe (for $B \gtrsim B_Q$). HL03 suggests that the absence of lines in the observed thermal spectra of several AXPs may be an indication of the vacuum polarization effect at work in these systems.

In our previous studies, as well as in other previous studies of magnetized hydrogen and helium NS atmospheres (see Pavlov et al. 1995; Zavlin & Pavlov 2002), the atmospheres are assumed to be completely ionized. Because the strong magnetic field significantly increases the binding energies of atoms, molecules, and other bound states (see Lai 2001 for a review), these bound states may have abundances appreciable enough to contribute to the opacity in the atmosphere (see Lai & Salpeter 1997; Potekhin, Chabrier, & Shibanov 1999). Although the energy levels and radiative transitions of a stationary H atom in strong magnetic fields have long been understood (e.g., Ruder et al. 1994), complications arise from the non-trivial effect of the center-of-mass motion of the atom on its internal structure (e.g., Potekhin 1998, and references therein). Also, because of the relatively high atmosphere density ($\rho \gtrsim 1 \text{ g cm}^{-3}$), a proper treatment of pressure ionization is important (e.g., Lai & Salpeter 1995; Potekhin et al. 1999). Recently, thermodynamically consistent equation of state (EOS) and opacities for a magnetized, partially ionized H plasma have been obtained by Potekhin & Chabrier (2003, hereafter PC). In this paper, we study NS atmosphere models based on the EOS and opacities of PC (see Ho et al. 2003 for an initial report of the results shown here).

Section 2 briefly summarizes the energy structure of hydrogen atoms in strong magnetic fields. Some details of the atmosphere models are discussed in Section 3. We present atmosphere models and spectra for different magnetic field strengths and temperatures in Section 4. In Section 5, we examine a dense plasma effect not accounted for in previous modeling of NS atmospheres. Section 6 summarizes and discusses the implications of our results.

2. HYDROGEN ATOM IN STRONG MAGNETIC FIELDS

In a strong magnetic field with $b = B/B_0 \gg 1$, where $B_0 = m_e^2 e^3 c / \hbar^3 = 2.3505 \times 10^9 \text{ G}$, the magnetic field confines the electron gyromotion in the transverse direction to a size $\sim a_0 / \ln b$, where a_0 is the Bohr radius, and the electron is restricted to the ground Landau level. The hydrogen atom energy spectrum is then specified by two quantum numbers (s, ν) , where s measures the mean transverse separation between the electron and proton (or the guiding center distance of the electron gyromotion) and ν gives the number of nodes in the z wave function. For $\ln[b/(2s+1)] \gg 1$, the energy of the states with $\nu = 0$ is $E_s^0 = -\mathcal{A}_s(\ln b)^2$, where the superscript “0” indicates the energy of an atom with a non-moving (infinitely massive) nucleus and \mathcal{A}_s depends weakly on b and s and formally tends to 1 Ry (= 13.6 eV) at $b \rightarrow \infty$. For example, for $s = 0$ and $10^{11} \text{ G} < B < 10^{16} \text{ G}$, $\mathcal{A}_s = (5.0 \pm 0.7) \text{ eV}$. A convenient fitting formula for arbitrary B (accurate to

within a few parts in 10^3 for $B < 10^{17} \text{ G}$ and $s \leq 3$) is

$$E_s^0 = -\mathcal{A}_s x^2, \quad x = \ln(1 + c_0 b), \quad (1)$$

$$\frac{\mathcal{A}_s}{\text{Ry}} = \frac{1 + c_2 x^{-2} + c_3 x^{-3} + c_5 x^{-5} + c_6 (1 + s)^{-2} x^{-6}}{1 + c_1 x^{-1} + c_4 x^{-2} + c_6 x^{-4}}. \quad (2)$$

Here, $c_5 = c_6(1 + s)/c_0$ ensures the correct behavior of the fit at $b \ll 1$, and the parameters c_i ($i = 0, 1, 2, 3, 4, 6$) are given in Table 1 for $s = 0, 1, 2, 3$.

For the states with $\nu > 0$, the energies at $b \gg 1$ are $E_{s\nu}^0 \simeq n^{-2} \text{ Ry}$, where n is the integer part of $(\nu + 1)/2$ (see Lai 2001, and references therein; see also Potekhin 1998 for a more comprehensive set of fitting formulae).

This simple picture of the H energy levels is modified when a finite proton mass is taken into account. Even for a “stationary” H atom, the energy E_s becomes $E_s^0 + s\hbar\omega_{Bp}$, where $\hbar\omega_{Bp} = 6.3 B_{12} \text{ eV}$ is the proton cyclotron energy and $B_{12} = B/(10^{12} \text{ G})$; the extra “proton recoil” energy $s\hbar\omega_{Bp}$ becomes increasingly important with increasing B . Moreover, the effect of center-of-mass motion is non-trivial: When the atom moves perpendicular to the magnetic field, a strong electric field is induced in its rest frame and can significantly change the atomic structure. Indeed, in the limit of large transverse pseudomomentum p_\perp , the atom assumes a decentered configuration, and its energy depends on p_\perp as $-p_\perp^{-1}$ rather than the usual p_\perp^2 dependence (see Potekhin 1998 for fitting formulae and references).

The most important transitions for the radiative opacity are the bound-free transition from the $(s, \nu) = (0, 0)$ state and the bound-bound transition $(0, 0) \rightarrow (1, 0)$. The former produces an absorption edge at the energy E_0^0 , which is smoothed out due to the dependence of E_0 on p_\perp from magnetic broadening (see Potekhin & Pavlov 1997) and due to the merging with transitions to $\nu > 0$ states at slightly lower energies (PC). The $(0, 0) \rightarrow (1, 0)$ transition produces the maximum absorption at the energy $E_0(p_\perp = 0) - E_1(p_\perp = 0) = E_0^0 - E_1^0 + \hbar\omega_{Bp}$; with increasing p_\perp , $E_0(p_\perp) - E_1(p_\perp)$ first decreases to a minimum and then increases to $\hbar\omega_{Bp}$. As a result, this bound-bound transition produces a magnetically broadened feature that resembles an inverted absorption edge, rather than a line, plus peaks at $\min(E_0 - E_1)$ and $\hbar\omega_{Bp}$ (Pavlov & Potekhin 1995). The transitions from $s = 0$ to $s > 1$ are forbidden for stationary atoms but become allowed for moving atoms and thus contribute to the opacity. See PC for more detailed discussion of opacity features.

3. MODEL METHOD

All models considered in this paper have the magnetic field aligned perpendicular to the stellar surface, and thus the spectra presented are emission from a local patch of the NS surface. We solve the full, angle-dependent radiative transfer equations for the two coupled photon modes in order to construct self-consistent NS atmosphere models. The two photon polarization modes in the magnetized plasma that characterizes NS atmospheres are the extraordinary mode (X-mode), which is mostly polarized perpendicular to the $\hat{k} - \hat{B}$ plane, and the ordinary mode (O-mode), which is mostly polarized parallel to the $\hat{k} - \hat{B}$ plane, where \hat{k} specifies the direction of photon propagation and \hat{B} is the direction of the external magnetic field. In our models, the temperature corrections $\Delta T(\tau)$

TABLE 1
PARAMETERS FOR ENERGY LEVELS OF HYDROGEN ATOM [SEE Eqs. (1) AND (2)]

s	c_0	c_1	c_2	c_3	c_4	c_6
0	1	20.62	27.37	164.19	106.0	1175.6
1	5	19.57	19.72	212.0	495.5	1903.7
2	12	12.53	13.02	207.8	907.9	1532.6
3	21	3.393	8.177	203.6	1313.8	1140.1

at each Thomson depth τ are applied iteratively until $\Delta T(\tau)/T(\tau) \lesssim 1\%$, deviations from radiative equilibrium are $\lesssim 1\%$, and deviations from constant flux are $\lesssim 2\%$ (see HL01 for details of our numerical method).

For the high magnetic field models (Section 4.2), we include the effect of vacuum polarization. As shown previously (Lai & Ho 2002, hereafter LH02), vacuum polarization induces conversion between the low-opacity mode and the high-opacity mode, and the efficiency of mode conversion depends on the photon energy. In the absence of a rigorous treatment of this effect, we follow HL03 by considering the two limiting cases: complete mode conversion (Section 4.2.2) and no mode conversion (Section 4.2.3). Our treatment of the no mode conversion case improves upon that given in HL03.

A major complication when incorporating bound species in the atmosphere models arises from the strong coupling between the center-of-mass motion of the atom and the internal atomic structure. PC have constructed thermodynamically consistent EOS and opacity models of partially ionized hydrogen plasmas in strong magnetic fields. From the work of PC, we obtain tables for the EOS and absorption opacities of hydrogen. The EOS tables for a given magnetic field are arranged by temperature and density. The pressure at Thomson depth τ ($= - \int \rho \kappa_0^{\text{es}} dz$, where $\kappa_0^{\text{es}} = \sigma_T/m_p$) is calculated from hydrostatic equilibrium. With a given temperature profile, we search the EOS tables for the nearest temperatures and pressures and do a weighted average to obtain the density profile. We also extract the atomic fraction from the EOS tables.

The opacity tables contain the absorption opacity $\kappa_\alpha^{\text{abs}}$ (where $\alpha = 0, \pm$) as a function of temperature, density, and photon energy. The absorption opacity for the modes ($j = 1$ for X-mode, $j = 2$ for O-mode) is obtained from

$$\kappa_j^{\text{abs}} = \sum_\alpha |e_\alpha^j|^2 \kappa_\alpha^{\text{abs}}, \quad (3)$$

where $e_0^j = e_z^j$ is the z-component (along \hat{B}) of the mode eigenvector and $e_\pm^j = (e_x^j \pm ie_y^j)/\sqrt{2}$ are the circular components. We calculate the polarization eigenvectors e^j assuming that the medium is fully ionized since the abundance of bound species is very low for the cases considered here (see Section 4); this is not strictly correct, but the effect of a small amount of bound species on the polarization of the medium is not known at present (see Bulik & Pavlov 1996 for the case where the atmosphere is completely neutral).¹ For a given layer in the atmosphere model, which specifies a particular temperature and density, the opacity $\kappa_\alpha^{\text{abs}}(E)$ at a given energy E is obtained

¹ For all the models considered in this paper, the neutral fraction is less than a few percent.

² The width of the proton cyclotron line in all the partially ionized models is due to the finite energy grid of the models and not an indication of the true line width; the true width is narrower.

from the geometric average of the nearest two or three energies of the table and used to compute $\kappa_j^{\text{abs}}(E)$. The scattering opacities are computed by the same method as in HL01 and HL03.

4. RESULTS

4.1. Low-Field ($B < B_Q$) Models

We consider three H atmosphere models in this subsection: $B_{12} = 1, T_{\text{eff},6} = T_{\text{eff}}/(10^6 \text{ K}) = 0.5$; $B_{12} = 1, T_{\text{eff},6} = 1$; $B_{12} = 10, T_{\text{eff},6} = 1$. Figure 1 shows the temperature and atomic fraction profiles as a function of density. The atomic fraction is the number of H atoms with non-destroyed energy levels divided by the total number of protons (see PC). The dependence of the atomic fraction on temperature and magnetic field is evident; in particular, lower temperatures or higher magnetic fields increase the abundance of bound species, with a maximum of a few percent for the models shown here.

Figure 2 shows the angle-averaged X-mode absorption opacity K_X^{abs} , defined by

$$K_X^{\text{abs}} = \frac{1}{4\pi} \int d\hat{k} \kappa_X^{\text{abs}}(\hat{k}). \quad (4)$$

as a function of energy for various temperatures and densities typical of the atmosphere models considered here. Even though the bound species abundance is very low, Fig. 2 shows that they can still have a very strong influence on the opacities. Besides the proton cyclotron line at $E_{Bp} = 6.3B_{12}$ eV, there are several strong features due to bound-bound and bound-free transitions. These are the $s = 0$ to $s = 1$ transition at $E = 51$ eV for $B_{12} = 1$ and at 0.14 keV for $B_{12} = 10$, the $s = 0$ to $s = 2$ transition at $E = 75$ eV for $B_{12} = 1$ and at 0.23 keV for $B_{12} = 10$, and the bound-free transition at $E = 161$ eV for $B_{12} = 1$ and at 0.31 keV for $B_{12} = 10$. Because of magnetic broadening (see Section 2), these features resemble bumps rather than ordinary spectral lines.

Figure 3 shows the spectra of the three atmosphere models. For comparison, we also show the spectra of the fully ionized models at the same B and T_{eff} , along with the non-magnetic fully ionized models at the same T_{eff} and the blackbody spectrum with $T = T_{\text{eff}}$. The proton cyclotron line at $E_{Bp} = 6.3B_{12}$ eV is clear in both the fully ionized and partially ionized spectra.² At $B \lesssim B_Q$, the effect of vacuum polarization on the atmosphere structure and spectra is weak; therefore there is no suppression of the proton cyclotron line (see Section 4.2 and HL03), and the proton cyclotron line can be very broad, especially when

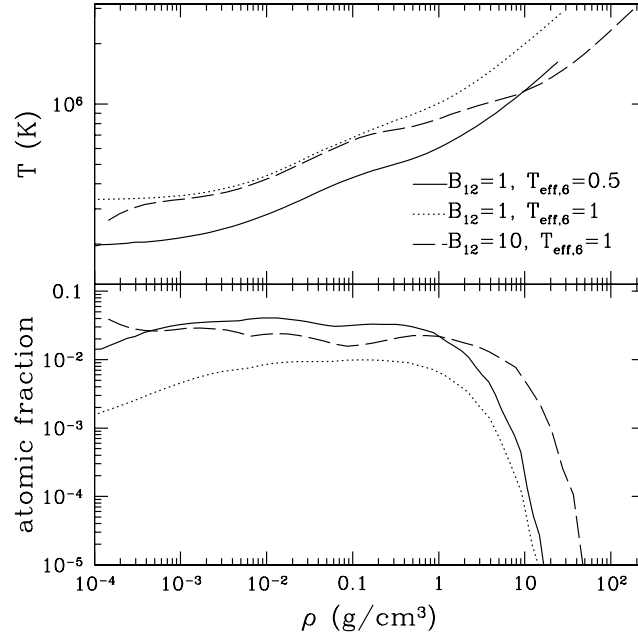


FIG. 1.— Temperature (upper panel) and atomic fraction (lower panel) as functions of density for various partially ionized H atmosphere models discussed in Section 4.1: magnetic field $B = 10^{12}$ G and effective temperature $T_{\text{eff}} = 5 \times 10^5$ K (solid lines), $B = 10^{12}$ G and $T_{\text{eff}} = 10^6$ K (dotted lines), and $B = 10^{13}$ G and $T_{\text{eff}} = 10^6$ K (dashed lines). Atomic fraction is the number of H atoms with non-destroyed energy levels divided by the total number of protons.

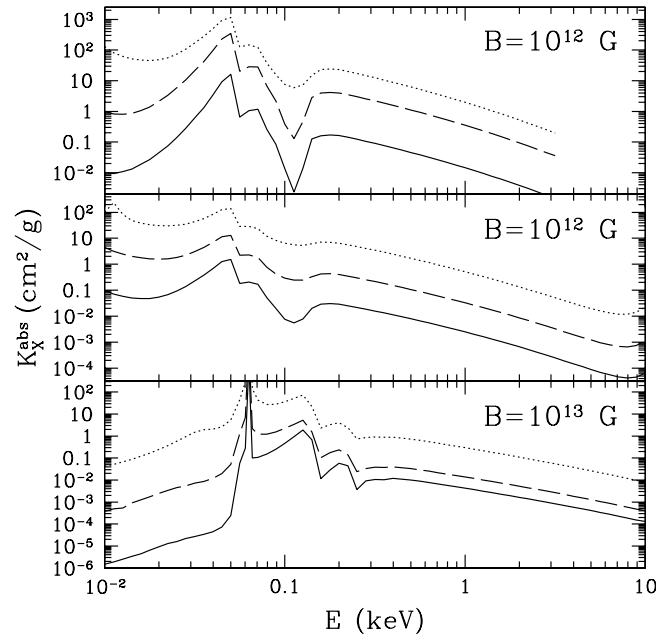


FIG. 2.— Angle-averaged X-mode absorption opacity K_X^{abs} as a function of energy for temperatures and densities representative of the atmosphere models discussed in Section 4.1. The upper panel shows K_X^{abs} appropriate for the model with magnetic field $B = 10^{12}$ G and effective temperature $T_{\text{eff}} = 5 \times 10^5$ K — $T = 4.2 \times 10^5$ K and $\rho = 0.093 \text{ g cm}^{-3}$ (dotted line), $T = 2.4 \times 10^5$ K and $\rho = 4.0 \times 10^{-3} \text{ g cm}^{-3}$ (dashed line), $T = 2.0 \times 10^5$ K and $\rho = 1.9 \times 10^{-4} \text{ g cm}^{-3}$ (solid line). The middle panel shows K_X^{abs} appropriate for the model with $B = 10^{12}$ G and $T_{\text{eff}} = 10^6$ K — $T = 7.4 \times 10^5$ K and $\rho = 0.16 \text{ g cm}^{-3}$ (dotted line), $T = 6.3 \times 10^5$ K and $\rho = 0.061 \text{ g cm}^{-3}$ (dashed line), $T = 4.3 \times 10^5$ K and $\rho = 8.7 \times 10^{-3} \text{ g cm}^{-3}$ (solid line). The lower panel shows K_X^{abs} appropriate for the model with $B = 10^{13}$ G and $T_{\text{eff}} = 10^6$ K — $T = 8.4 \times 10^5$ K and $\rho = 1.0 \text{ g cm}^{-3}$ (dotted line), $T = 6.2 \times 10^5$ K and $\rho = 0.061 \text{ g cm}^{-3}$ (dashed line), $T = 3.5 \times 10^5$ K and $\rho = 1.1 \times 10^{-3} \text{ g cm}^{-3}$ (solid line). The opacity curves in each panel are in descending order from hotter and higher density to cooler and lower density, and the upper K_X^{abs} (dotted) curves have been multiplied by 10 while the lower K_X^{abs} (solid) curves have been divided by 10 for clarity. See text for description of the opacity features.

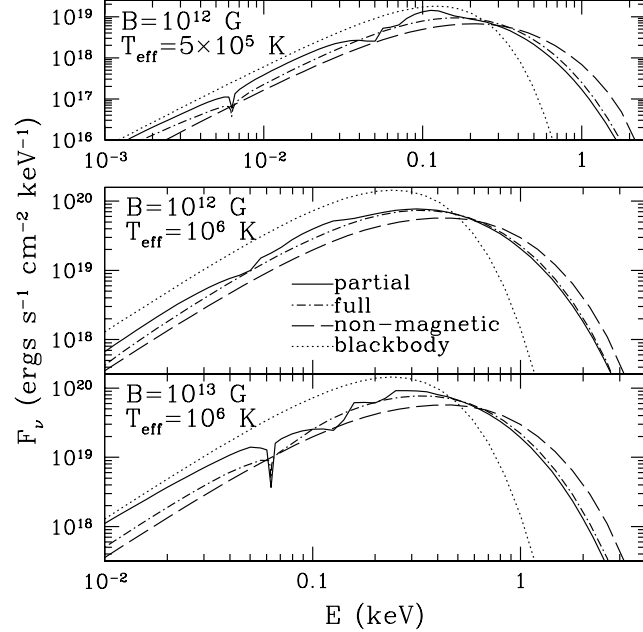


FIG. 3.— Spectra of hydrogen atmospheres with $B = 10^{12}$ G and $T_{\text{eff}} = 5 \times 10^5$ K (upper panel), $B = 10^{12}$ G and $T_{\text{eff}} = 10^6$ K (middle panel), and $B = 10^{13}$ G and $T_{\text{eff}} = 10^6$ K (lower panel). The solid line is for a partially ionized atmosphere, the dot-dashed line is for a fully ionized atmosphere, the dashed line is for a fully ionized non-magnetic atmosphere, and the dotted line is for a blackbody with $T = T_{\text{eff}}$. The proton cyclotron line in the partially ionized spectra is not resolved (see footnote 2).

$E_{Bp} \gtrsim 3kT_{\text{eff}}$ (HL01). A comparison of the $B = 10^{12}$ G models shows that spectral features due to neutral species in the atmosphere are weaker in the higher temperature model. This is because the higher temperatures decreases the abundance of neutral species (see Fig. 1) and thus reduces the effect of the neutral species on the continuum opacity.

It is evident from Fig. 3 that spectral features due to bound species at these field strengths lie within the extreme UV to very soft X-ray ($50 \text{ eV} \lesssim E \lesssim 200 \text{ eV}$) regime and therefore are difficult to observe due to interstellar absorption. However, the effect of bound species on the temperature profile of the atmosphere and the continuum flux is significant. In particular, the optical flux is higher for the partially ionized atmospheres compared to the fully ionized atmospheres. On the other hand, the partially and fully ionized models both yield very similar (neglecting the spectral features) hard X-ray flux for a given effective temperature, with the partially ionized model fluxes slightly lower than those from the fully ionized models; thus fitting the observed hard X-ray flux with fully ionized models would yield fairly accurate NS temperatures.

4.2. Magnetar ($B > B_Q$) Models

When studying magnetar atmosphere models, it is important to include the effect of vacuum polarization. However, to clearly see the role of bound species, we first consider models in which vacuum polarization is neglected.

4.2.1. No Vacuum Polarization

Figure 4 shows the temperature and atomic fraction profiles for the H atmosphere model with $B_{14} = B/(10^{14} \text{ G}) = 5$ and $T_{\text{eff},6} = 5$. Here we use an extension of the PC EOS and opacity model to $B > 10^{13.5}$ G.

In this case, instead of the fits of Potekhin (1998) employed in PC (some of which would fail at $B \gtrsim 10^{13.5}$ G), we perform numerical calculations of the atomic energies, sizes, and oscillator strengths following Potekhin (1994). (Some results of this extension of the PC model have been reported in Chabrier, Douchin, & Potekhin 2002.) Though the magnetic field increases the binding energy of the hydrogen atom to > 0.5 keV, the atomic abundance remains $< 1\%$ in the atmospheric layers.

The upper panel of Figure 5 shows the angle-averaged X-mode opacity K_X^{abs} as a function of energy for various temperatures and densities typical of the high magnetic field model considered here. Besides the proton cyclotron line at $E_{Bp} = 0.63 B_{14}$ keV, the sharp change in opacity at 0.76 keV for $B_{14} = 5$ is due to photoionization. The features at $E > E_{Bp}$ are the partial photoionization edges for transitions to the continuum states with $s > 0$, which are merged with autoionization resonances just below the corresponding partial thresholds and extended redwards due to magnetic broadening (see Potekhin & Pavlov 1997). The bound-bound transitions are not seen in Fig. 5 because the bound states with $s > 0$ merge with the continuum at such field strengths because of the $s\hbar\omega_{Bp}$ -term in E_s .

Figure 6 shows the spectra of the models with $B = 5 \times 10^{14}$ G and $T_{\text{eff}} = 5 \times 10^6$ K. The upper panel is a comparison of partially and fully ionized models with no vacuum polarization. Broad absorption features at $E \sim 0.76$ keV and 4 keV are due to bound-free transitions to different continuum states (the latter feature is from the blending of two magnetically broadened partial photoionization edges at 3.4 keV and 6.5 keV; see Fig. 5), while the continuum flux between the models is not significantly different. Also, as noted in HL01 and HL03 (see

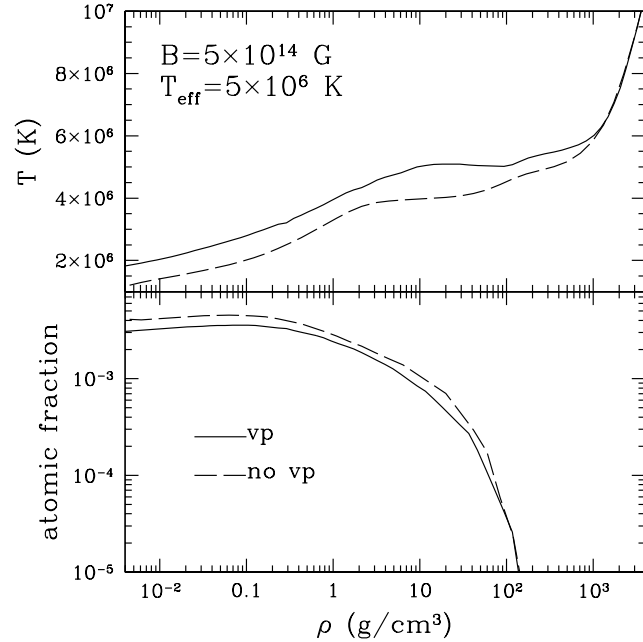


FIG. 4.— Temperature (upper panel) and atomic fraction (lower panel) as functions of density for the partially ionized H atmosphere models discussed in Section 4.2: $B = 5 \times 10^{14}$ G and $T_{\text{eff}} = 5 \times 10^6$ K with vacuum polarization (solid lines) and without vacuum polarization (dashed lines). Atomic fraction is the number of H atoms with non-destroyed energy levels divided by the total number of protons.

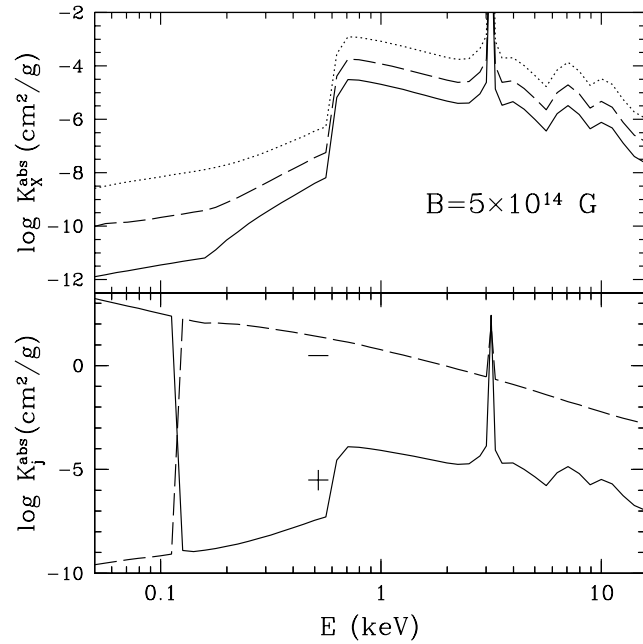


FIG. 5.— Angle-averaged absorption opacities as functions of energy for temperatures and densities representative of the $B = 5 \times 10^{14}$ G and $T_{\text{eff}} = 5 \times 10^6$ K atmosphere model including vacuum polarization discussed in Section 4.2. The upper panel shows the X-mode opacity K_X^{abs} at $T = 2.9 \times 10^6$ K and $\rho = 0.13 \text{ g cm}^{-3}$ (dotted line), $T = 2.4 \times 10^6$ K and $\rho = 0.031 \text{ g cm}^{-3}$ (dashed line), $T = 1.8 \times 10^6$ K and $\rho = 4.0 \times 10^{-3} \text{ g cm}^{-3}$ (solid line). The opacity curves in the upper panel are in descending order from hotter and more dense to cooler and lower density, and the upper K_X^{abs} (dotted) curves have been multiplied by 10 while the lower K_X^{abs} (solid) curves have been divided by 10 for clarity. The lower panel shows the plus-mode and minus-mode opacities K_j^{abs} ($j = \pm$) and T and ρ corresponding to the dotted curve in the upper panel; using K_+^{abs} and K_-^{abs} is appropriate for models in which complete mode conversion is assumed (see Section 4.2.2). See text for description of the opacity features.

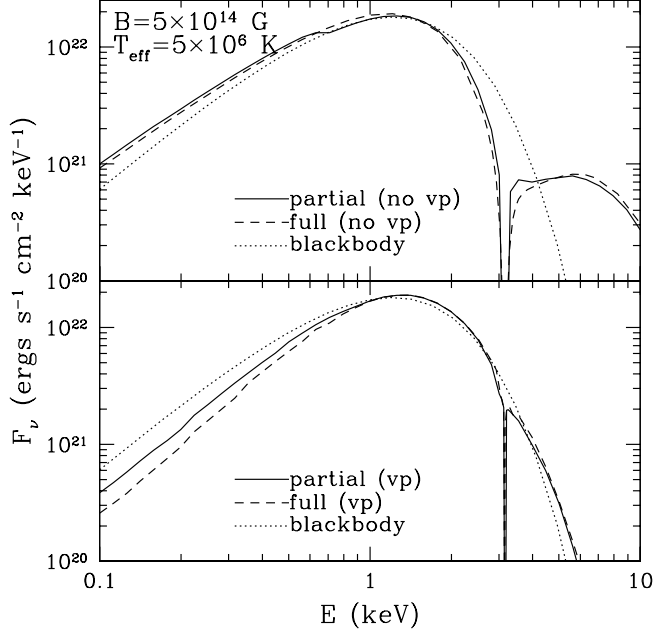


FIG. 6.— Spectra of hydrogen atmospheres with $B = 5 \times 10^{14}$ G and $T_{\text{eff}} = 5 \times 10^6$ K. The upper panel shows the partially ionized (solid line) and fully ionized (dashed line) atmospheres with no vacuum polarization. The lower panel shows the partially ionized (solid line) and fully ionized (dashed line) atmospheres with vacuum polarization and assuming complete mode conversion. The dotted lines are for a blackbody with $T = 5 \times 10^6$ K. The proton cyclotron line in the partially ionized spectra is not resolved (see footnote 2).

also Zane et al. 2001), the proton cyclotron line is very broad when vacuum polarization is neglected.

4.2.2. Including Vacuum Polarization: Complete Mode Conversion

The main effect of vacuum polarization on radiative transfer is the “vacuum resonance,” which occurs when the effects of the vacuum and plasma on the polarization modes cancel each other. For a photon of energy $E (= \hbar\omega)$, the vacuum resonance occurs at density

$$\rho_V \approx 0.96 Y_e^{-1} E_1^2 B_{14}^2 f(B)^{-2} \text{ g cm}^{-3}, \quad (5)$$

where $E_1 = E/(1 \text{ keV})$ and $f(B)$ is a slowly-varying function of B of order unity. The two photon modes are almost linearly polarized away from the resonance, while they both become circularly polarized near ρ_V . LH02 showed that a photon propagating in the atmospheric plasma can adiabatically convert from the low-opacity X-mode to the high-opacity O-mode (and vice versa) as it crosses ρ_V . For this conversion to be effective, the adiabatic condition

$$E_{\text{ad}} \gtrsim 1.49 [f(B) \tan \theta_B |1 - u_i|]^{2/3} (5 \text{ cm}/H_\rho)^{1/3} \text{ keV}, \quad (6)$$

where θ_B is the angle between \hat{k} and \hat{B} , $u_i = \omega_{Bp}^2/\omega^2$, and $H_\rho = |dz/d\ln \rho|$ is the density scale height along the ray, must be satisfied. Clearly, resonant mode conversion can significantly affect radiative transfer (LH02; HL03; Lai & Ho 2003).

To rigorously treat the radiative transfer across the vacuum resonance, one must go beyond the modal description of the radiation field by solving the transfer equation in terms of the photon intensity matrix (Lai & Ho 2003). In the present paper, as in HL03, we consider two limiting cases. In the “complete mode conversion” case, we

assume photons of all energies change their mode characteristics (from X to O-mode or vice versa) when crossing the vacuum resonance. This can be achieved by using the plus-mode and minus-mode basis ($j = \pm$) in the radiative transfer equation (see HL03 for details). At a given density ρ , the characteristics of the \pm -modes switch at the energy

$$E_V \approx 1.02 Y_e^{1/2} \rho_1^{1/2} B_{14}^{-1} f(B) \text{ keV}, \quad (7)$$

where $\rho_1 = \rho/(1 \text{ g cm}^{-3})$.

Figure 4 shows the temperature and atomic fraction profiles for the partially ionized model which includes vacuum polarization in the complete mode conversion limit. As noted in HL03, vacuum polarization increases the temperature at each depth relative to the case without vacuum polarization. The higher temperatures result in lower atomic fractions for a given magnetic field.

The lower panel of Fig. 5 shows the angle-averaged opacity K_j^{abs} for $j = \pm$ as a function of energy at $\rho = 0.13 \text{ g cm}^{-3}$ and $T = 2.9 \times 10^6$ K, which are characteristic of the $B = 5 \times 10^{14}$ G atmosphere. The distinction between the plus and minus-modes ($j = \pm$) and the X and O-modes is discussed in HL03 (in particular, see Fig. 4 of that work). At this particular temperature and density, the plus-mode (minus-mode) is in the high (low) opacity state for $E < E_V$ but manifests as the low (high) opacity state for $E > E_V$.

Fig. 6 compares the spectra of different models with and without vacuum polarization. First, we see that, with vacuum polarization, the continuum flux at high energies for the partially ionized model is very similar to the fully ionized model [for the parameters shown in Fig. 6, $F_\nu(\text{partial})/F_\nu(\text{full}) < 1.5$ at $E > 0.1 \text{ keV}$]. Second, vacuum polarization softens the high energy tail of the spec-

trum in both the partially ionized and fully ionized cases, although the emission is still harder than the blackbody spectrum because of the non-grey opacities. The softer spectrum is due to the density dependence of the vacuum resonance energy E_V and the large density gradient present in the atmosphere; the change in opacity at the vacuum resonance causes the high energy photons emerging from the atmosphere to be produced from a shallower, cooler layer in the atmosphere than in the case when vacuum polarization is neglected (see Fig. 2 of Ho et al. 2003). Third, as discussed in HL03, this vacuum-induced depression of continuum flux strongly suppresses the proton cyclotron line by making the photospheres inside and outside the line more similar (see also footnote 2). We now see that vacuum polarization also suppresses spectral features due to the bound species of hydrogen. The reduced width of the proton cyclotron line and spectral features associated with bound transitions makes these features difficult to observe with current X-ray detectors (see Section 6).

4.2.3. Including Vacuum Polarization: No Mode Conversion

The opposite limit for treating the vacuum polarization effect is to assume no mode conversion across ρ_V . This is achieved by using the X-mode and O-mode as the mode basis in the transfer equation (see HL03). For this case, the X-mode opacity has a much lower opacity than the O-mode opacity except at the resonance peak $E = E_V$ (where $\kappa_X = \kappa_O$). As discussed in LH02, even without mode conversion, the optical depth across this opacity feature can be significant; therefore, the X-mode radiative transfer is affected.

We present here improvements made to our models with no mode conversion. The atmosphere models contain energy grid points E_n and density grid points ρ_i . As described in HL03, we use an adaptive energy grid to account for the narrow, density-dependent opacity feature at E_V , i.e., an equal number of density and energy grid points is used with every energy grid point being placed at $E_n = E_V(\rho_i)$. We noted in HL03, however, that this implementation overestimates the strength of the opacity feature on the atmosphere structure and spectra. This is illustrated in Figure 7: The area under the short-dashed line overestimates the area under the solid line, which represents the true opacity.

To rectify this problem, we introduce an effective opacity at the resonance, $\bar{\kappa}(E_V)$, given by

$$\begin{aligned} \bar{\kappa}(E_n = E_V) = & \frac{2}{E_{n+1} - E_{n-1}} \left[\int_{E_{n-1}}^{E_{n+1}} \kappa(E) dE \right. \\ & - \frac{1}{2} \kappa(E_{n-1}) (E_n - E_{n-1}) \\ & \left. - \frac{1}{2} \kappa(E_{n+1}) (E_{n+1} - E_n) \right], \end{aligned} \quad (8)$$

where the integral is calculated using an auxiliary energy grid that has much finer resolution. Using $\bar{\kappa}(E_V)$ preserves the equivalent width of the resonance feature: In Fig. 7, the area under the long-dashed line is equal to the area under the solid line. As would be expected, atmosphere models based on this improved method but with different numbers of energy grid points yield very similar results.

The spectra for fully ionized hydrogen atmosphere models with $B = 5 \times 10^{14}$ G and $T_{\text{eff}} = 5 \times 10^6$ K is shown in Figure 8. Note that the width of the proton cyclotron line in the (no mode conversion) adaptive energy grid models is not the true width of the line. The broad depression in the spectrum due to the density dependence of the vacuum resonance feature is shifted to higher energies since the old calculation (see HL03) overestimated the effect of the resonance feature. The two limiting cases of complete mode conversion and no mode conversion should approximately bracket the true spectrum. We also note that the no mode conversion flux spectrum should be suppressed at low energies due to the dense plasma effect described in Section 5, and thus the two limiting cases should have more similar fluxes at lower energies than is shown in Figure 8.

4.2.4. Proper Treatment of Free-Free Opacity

As discussed in PC, the traditional formula (see Pavlov et al. 1995) for the opacity due to free-free absorption of both electrons and ions given by

$$\kappa_{\alpha}^{\text{ff}} \propto \frac{1}{(\omega + \alpha\omega_{Be})^2} + \left(\frac{m_e}{m_p} \right)^2 \frac{1}{(\omega - \alpha\omega_{Bp})^2} \quad (\text{incorrect}), \quad (9)$$

where $\alpha = 0, \pm 1$ and $\hbar\omega_{Be} = 11.6 B_{12}$ keV is the electron cyclotron energy, misses an interference effect due to electron-ion collisions. The correct free-free absorption opacity is given by (see, e.g., PC for more discussion)

$$\kappa_{\alpha}^{\text{ff}} \propto \frac{\omega^2}{(\omega + \alpha\omega_{Be})^2 (\omega - \alpha\omega_{Bp})^2} \quad (\text{correct}). \quad (10)$$

When $\omega \gg \omega_{Bp}$, equations (9) and (10) are very nearly the same. However, when $\omega < \omega_{Bp}$, the correct opacity is suppressed by a factor $\sim \omega^2/\omega_{Bp}^2$ compared to the incorrect one. Thus we expect that, in the atmosphere models using the correct opacity given by equation (10), the photons with $E < E_{Bp}$ will be generated from deeper, hotter layers as opposed to models which use the incorrect opacity given by equation (9). All previous atmosphere models adopted equation (9) and are therefore problematic if photons with $E < E_{Bp}$ are important (see, however, Lloyd 2003).

Figure 9 compares atmosphere spectra generated using the correct expression for the free-free absorption opacity [eq. (10)] and using the incorrect expression [eq. (9)]. The model shown here is a more extreme example since $E_{Bp} \gtrsim kT_{\text{eff}}$ (in order to maintain constant total flux, a large redistribution of the specific energy flux occurs). When $E_{Bp} \ll kT_{\text{eff}}$, such as for the low magnetic field cases considered in Section 4.1, the difference between using the correct expression versus the incorrect one is small (except possibly in the region $\omega < \omega_{Bp}$; but this region of the spectrum carries negligible flux). All models considered in this paper use the correct expression.

5. DENSE PLASMA EFFECT

Here we comment on a main uncertainty associated with atmosphere models of strongly magnetized NSs. Although we have included the medium effect on the polarization modes, at sufficiently high densities or low photon energies, the refractive index of the medium deviates appreciably from unity. In particular, at the photon decoupling layer in the atmosphere (where the optical depth

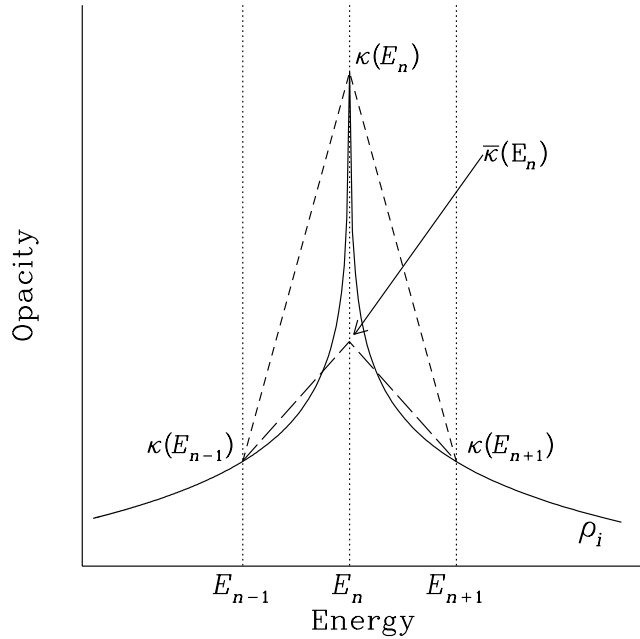


FIG. 7.— Schematic picture of the radiative opacity as a function of energy at the density grid point ρ_i . The vacuum resonance feature occurs at higher energies at larger densities (depths) [see eq. (7)]. In the adaptive energy grid method of HL03 and Section 4.2.3, the energy grid points E_{n-1}, E_n, E_{n+1} are chosen to be equal to the vacuum resonance energy at one of the density grid points, i.e., $E_n = E_V(\rho_i)$. The short-dashed line indicates the apparent opacity obtained by interpolating energy grid points E_{n-1}, E_n, E_{n+1} , while the long-dashed line indicates the apparent opacity obtained by the method described in Section 4.2.3.

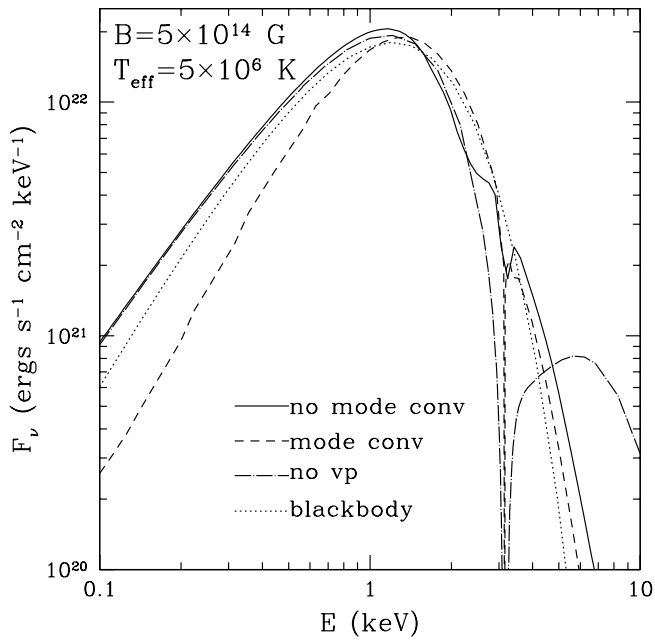


FIG. 8.— Spectra of fully ionized hydrogen atmospheres with $B = 5 \times 10^{14}$ G and $T_{\text{eff}} = 5 \times 10^6$ K. The solid line and dashed line are the atmospheres with vacuum polarization but no mode conversion and complete mode conversion, respectively, the dot-dashed line is the atmosphere without vacuum polarization, and the dotted line is for a blackbody with $T = 5 \times 10^6$ K.

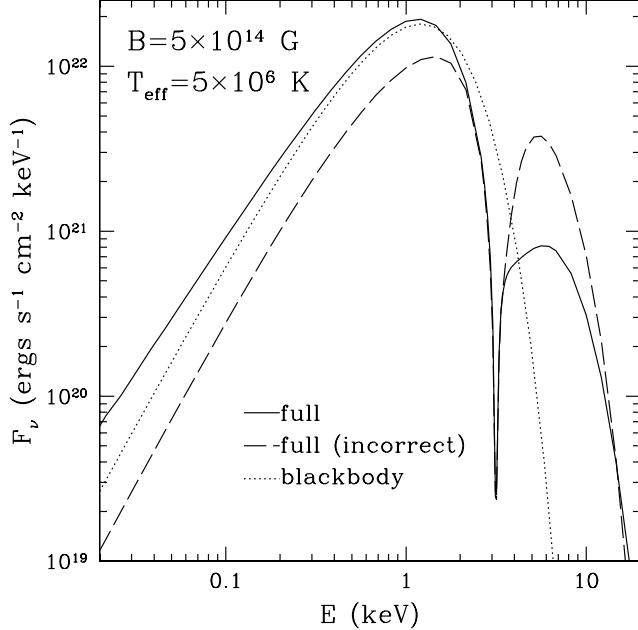


FIG. 9.— Spectra of fully ionized hydrogen atmospheres with $B = 5 \times 10^{14}$ G and $T_{\text{eff}} = 5 \times 10^6$ K using the correct (solid) expression for the free-free absorption opacity [eq. (10)] versus the incorrect (dashed) expression [eq. (9)]. The dotted line is for a blackbody with $T = 5 \times 10^6$ K.

$\tau_{\nu} \approx 1$), the plasma frequency ω_{pe} may exceed the photon frequency ω . For example, in the $B = 10^{12}$ G and $T_{\text{eff}} = 5 \times 10^5$ K model shown in Section 4.1, the X-mode photons (which are the main carriers of the energy flux) with $E \lesssim 10$ eV decouple from the atmosphere layer where $E < \hbar\omega_{\text{pe}} = 28.71 (\rho/1 \text{ g cm}^{-3})^{1/2}$ eV (see lower panel of Fig. 10). Clearly we expect that the actual emission at these energies is lower than what is shown in our model spectrum (see upper panel of Fig. 3).

A quantitative study of this dense plasma effect is beyond the scope of this paper. However, we can obtain an estimate of its effect by a simple procedure. In the atmosphere model, we evaluate the parameter $v_e (= \omega_{\text{pe}}^2/\omega^2)$; whenever $v_e > 1$, we artificially increase all the opacities at that energy and depth by a factor $\gamma_p (\gg 1)$. This simulates the suppression of radiation below the plasma frequency cutoff. The resulting spectrum is shown in Fig. 10, where we have chosen $\gamma_p = 10^2$ and 10^4 and labeled the results as “dense.” The result of Section 4.1, where we “blindly” carry out the calculations even when $v_e > 1$, is labeled as “normal” in Fig. 10. We see that the spectrum is largely unaffected since $v_e < 1$ at most energies. However, we see the flux at low energies ($E \lesssim 5$ eV) is suppressed [with $F_{\nu}^{(\text{norm})}/F_{\nu}^{(\text{dense})} \approx 1.4$ at 2 eV for $\gamma_p = 10^2$ and $F_{\nu}^{(\text{norm})}/F_{\nu}^{(\text{dense})} \approx 1.7$ at 2 eV for $\gamma_p = 10^4$]. The slight increase in flux at $\sim 7\text{-}20$ eV is due to flux redistribution to maintain constant total flux or radiative equilibrium.

For the magnetar models, the strong suppression of the X-mode opacities by the magnetic field causes the photons to be generated from deeper, denser atmosphere layers. Therefore, the dense plasma effect may be even more important. (However, this can be offset by vacuum polarization which makes the photosphere shallower; see Section 4.2.) Clearly this dense plasma effect needs to be un-

derstood better before accurate comparisons can be made with, for example, optical and infrared observations.

6. DISCUSSION

We have presented results of the first magnetic hydrogen atmosphere models of isolated neutron stars based on the best current equation of state and opacities of magnetized, partially ionized H plasmas (PC). For models with “ordinary” magnetic field strengths ($10^{12} \text{ G} \lesssim B \lesssim B_Q = 4.4 \times 10^{13}$ G), the spectral lines associated with bound species lie in the extreme UV to very soft X-ray energy bands and are difficult to observe due to interstellar absorption at these energies (though a broad absorption feature at ~ 0.2 keV was seen in RBS 1223; Haberl et al. 2003; see also Ho & Lai 2003b). However, the opacities are sufficiently different from the fully ionized opacities that they can change the atmosphere structure and continuum flux.

We find that, for the higher magnetic field models ($B > B_Q$), vacuum polarization suppresses both the proton cyclotron line and spectral lines due to the bound species. As a result, the thermal spectra are almost featureless and blackbody-like. Recent observations of several AXPs with *Chandra* and *XMM-Newton* X-ray telescopes failed to resolve any significant line features in the spectra (e.g., Patel et al. 2001, 2003; Juett et al. 2002; Tiengo et al. 2002; Morii et al. 2003); thus this could possibly be indicating the presence of vacuum polarization effects in these magnetar candidates.

Our results may also be useful in understanding spectral observations of dim isolated neutron stars, such as RX J1856.5–3754 and RX J0720.4–3125 (see, e.g., Pavlov et al. 2002; Kaplan et al. 2003). Since $kT_{\text{eff}} \sim$ tens of eV for these neutron stars, the presence of neutral atoms must be accounted for in the atmosphere models if $B \gtrsim 10^{12}$ G. We find that one-temperature partially ionized hydro-

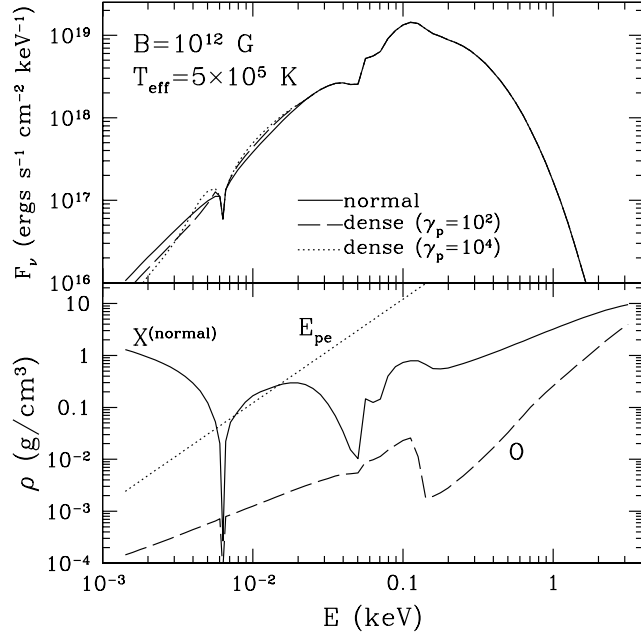


FIG. 10.— Spectra (upper panel) and density at the photosphere (lower panel) for partially ionized hydrogen atmospheres with $B = 10^{12}$ G and $T_{\text{eff}} = 5 \times 10^5$ K. In the upper panel, the solid line shows the spectrum (“normal”) when the dense plasma effect discussed in Section 5 is neglected, while the dashed line and dotted line show the spectra (“dense”) when the dense plasma effect is approximately accounted for using $\gamma_p = 10^2$ and 10^4 , respectively. The lower panel shows the density at the X-mode photon decoupling layer (at which $\tau_\nu \approx 1$; solid line) and the O-mode photon decoupling layer (dashed line). The dotted line denotes the density at which the photon frequency equals the plasma frequency, i.e., $E = \hbar\omega_{\text{pe}} = 28.71 \rho_1^{1/2}$ eV.

gen atmosphere models improve the fitting of the X-ray data (compared to fully ionized models), although they still do not provide a satisfactory fit to the combined X-ray and optical spectra. One possible solution is “thin” atmosphere models in which a gaseous hydrogen atmosphere lies on top of a condensed matter (see Motch et al. 2003). We find that the spectra of the neutron stars RX J1856.5 – 3754 and RX J0720.4 – 3125 can be crudely fit by our $B = 10^{12}$ G and $T_{\text{eff}} \sim 5 \times 10^5$ K partially ionized hydrogen “thin” atmosphere model (Ho et al., in preparation). The resulting optical spectrum of the model only overpredicts the optical data by $\lesssim 1.5$. Furthermore, when the dense plasma effect discussed in Section 5 is taken into account, the suppression of low energy flux may lead to an even better fit of the optical spectrum.

Chandra and *XMM-Newton* observations revealed absorption features at 0.7 and 1.4 keV in the spectra of the neutron star 1E 1207.4 – 5209 (Mereghetti et al. 2002b; Sanwal et al. 2002). Sanwal et al. (2002) contend the features are due to atomic transitions of singly-ionized helium in the neutron star atmosphere with a superstrong magnetic field, $B \approx 1.5 \times 10^{14}$ G. Hailey & Mori (2002) and Mori & Hailey (2003) attribute the features to transitions of mid- Z oxygen or neon in a $\sim 10^{12}$ G magnetic field, while Mereghetti et al. (2002b) interpret the features to be the result of high- Z metals at $\sim 10^{12}$ G. If 1E 1207.4 – 5209 is indeed a neutron star with superstrong magnetic field ($B \gtrsim B_{\text{Q}}$) and the properties of the helium atom are similar to those of the hydrogen atom at these field strengths, then our results show that any spectral features would not be resolved due to their suppression by vacuum polarization. However, we cannot be more definitive because of the

unknown properties of helium at these field strengths and, as discussed in Section 3, we assumed that the presence of a very small amount of neutral atoms has no effect on the polarization properties of the medium. Furthermore, recent observations have revealed an additional feature at 2.1 keV and possibly another at 2.8 keV thus hinting at an electron cyclotron origin (with $B = 8 \times 10^{10}$ G) for these features (Bignami et al. 2003).

Several caveats/uncertainties are worth mentioning. (1) The radiative transfer formalism adopted in our work relies on the transfer of two photon polarization modes. This is inadequate for treating the vacuum polarization-induced resonant mode conversion effect, especially because the effectiveness of mode conversion depends on photon energy (see LH02; HL03). To properly account for the mode conversion effect, as well as mode collapse and the breakdown of Faraday depolarization, one must go beyond the modal description of the radiation field by formulating and solving the transfer equation in terms of the photon intensity matrix (or Stokes parameters) and including the effect of a nontrivial refractive index (see Lai & Ho 2003). (2) As discussed in Section 5, the dense plasma effect on radiative transfer can be important, especially for low energy photons and high magnetic fields. These issues require further study.

We thank Marten van Kerkwijk for useful discussions and for also obtaining rough fits of our models to the spectra of RX J1856.5 – 3754 and RX J0720.4 – 3125. We thank the anonymous referee for useful comments. We are grateful to the Cornell Hewitt Computer Laboratory for the use of its facilities. This work is supported in part by

NASA grant NAG 5-12034 and NSF grant AST 0307252. A.Y.P. acknowledges the hospitality of the Cornell Astronomy Department, where part of this work was performed.

The work of A.Y.P. is supported by RFBR grants 02-02-17668 and 03-07-90200.

REFERENCES

Adler, S.L. 1971, *Ann. Phys.*, 67, 599
 Becker, W. 2000, in *Proc. IAU Symp. 195, Highly Energetic Physical Processes and Mechanisms for Emission from Astrophysical Plasmas*, eds. Martens, P.C.H., Tsuruta, S., & Weber, M.A. (San Francisco: ASP), p.49
 Bignami, G.F., Caraveo, P.A., De Luca, A., & Mereghetti, S. 2003, *Nature*, 423, 725
 Bulik, T. & Pavlov, G.G. 1996, *ApJ*, 469, 373
 Chabrier, G., Douchin, F., & Potekhin, A.Y. 2002, *J. Phys.: Condens. Matter*, 14, 9133
 Gnedin, Yu.N., Pavlov, G.G., & Shibanov, Yu.A. 1978, *Sov. Astron. Lett.*, 4, 117
 Haberl, F., Schweppe, A.D., Hambaryan, V., Hasinger, G., & Motch, C. 2003, *A&A*, 403, L19
 Hailey, C.J. & Mori, K. 2002, *ApJL*, 578, L133
 Heyl, J.S. & Hernquist, L. 1997, *Phys. Rev. D*, 55, 2449
 Ho, W.C.G. & Lai, D. 2001, *MNRAS*, 327, 1081 (HL01)
 Ho, W.C.G. & Lai, D. 2003a, *MNRAS*, 338, 233 (HL03)
 Ho, W.C.G. & Lai, D. 2003b, *ApJ*, to be submitted
 Ho, W.C.G., Lai, D., Potekhin, A.Y., & Chabrier, G. 2003, *Adv. Sp. Res.*, in press (astro-ph/0212077)
 Hurley, K. 2000, in *Gamma-Ray Bursts: Fifth Huntsville Symposium*, AIP Conf. Proc. 526, eds. Kippen, R.M., Mallozzi, R.S., & Fishman, G.J. (New York: AIP), p.515
 Juett, A.M., Marshall, H.L., Chakrabarty, D., & Schulz, N.S. 2002, *ApJL*, 568, L31
 Kaplan, D.L., Kulkarni, S.R., & van Kerkwijk, M.H. 2003, *ApJL*, 588, L33
 Lai, D. 2001, *Rev. Mod. Phys.*, 73, 629
 Lai, D. & Ho, W.C.G. 2002, *ApJ*, 566, 373 (LH02)
 Lai, D. & Ho, W.C.G. 2003, *ApJ*, 588, 962
 Lai, D. & Salpeter, E.E. 1995, *Phys. Rev. A*, 52, 2611
 Lai, D. & Salpeter, E.E. 1997, *ApJ*, 491, 270
 Lloyd, D. 2003, *MNRAS*, submitted (astro-ph/0303561)
 Mereghetti, S., Chiarlone, L., Israel, G.L., & Stella, L. 2002a, in *Proc. 270 WE-Heraeus Seminar on Neutron Stars, Pulsars, and Supernova Remnants*, eds. Becker, W., Lesch, H., & Trümper, J., (MPE Rep. 278; Garching: MPI), p.29
 Mereghetti, S., De Luca, A., Caraveo, P.A., Becker, W., Mignani, R., & Bignami, G.F. 2002b, *ApJ*, 581, 1280
 Mészáros, P. 1992, *High-Energy Radiation from Magnetized Neutron Stars* (Chicago: University of Chicago Press)
 Mészáros, P. & Ventura, J. 1979, *Phys. Rev. D*, 19, 3565
 Mori, K. & Hailey, C.J. 2003, *ApJ*, submitted (astro-ph/0301161)
 Mori, M., Sato, R., Kataoka, J., & Kawai, N. 2003, *PASJ*, 55, L45
 Motch, C., Zavlin, V.E., & Haberl, F. 2003, *A&A*, 408, 323
 Patel, S.K., et al. 2001, *ApJL*, 563, L45
 Patel, S.K., et al. 2003, *ApJ*, 587, 367
 Pavlov, G.G. & Gnedin, Yu.N. 1984, *Sov. Sci. Rev. E*, 3, 197
 Pavlov, G.G. & Potekhin, A.Y. 1995, *ApJ*, 450, 883
 Pavlov, G.G., Zavlin, V.E., & Sanwal, D. 2002, in *Proc. 270 WE-Heraeus Seminar on Neutron Stars, Pulsars, and Supernova Remnants*, eds. Becker, W., Lesch, H., & Trümper, J., (MPE Rep. 278; Garching: MPI), p.273
 Pavlov, G.G., Shibanov, Yu.A., Zavlin, V.E., & Meyer, R.D. 1995, in *Lives of the Neutron Stars*, eds. Alpar, M.A., Kiziloglu, Ü., & van Paradijs, J. (Boston: Kluwer), p.71
 Potekhin, A.Y. 1994, *J. Phys. B*, 27, 1073
 Potekhin, A.Y. 1998, *J. Phys. B*, 31, 49
 Potekhin, A.Y. & Chabrier, G. 2003, *ApJ*, 585, 955 (PC)
 Potekhin, A.Y. & Pavlov, G.G. 1997, *ApJ*, 483, 414
 Potekhin, A.Y., Chabrier, G., & Shibanov, Yu.A. 1999, *Phys. Rev. E*, 60, 2193
 Ruder, H., Wunner, G., Herold, H., & Geyer, F. 1994, *Atoms in Strong Magnetic Fields* (Berlin: Springer-Verlag)
 Sanwal, D., Pavlov, G.G., Zavlin, V.E., & Teter, M.A. 2002, *ApJL*, 574, L61
 Thompson, C. 2001, in *Neutron Star-Black Hole Connection*, eds. Kouveliotou, C., Ventura, J., & van den Heuvel, E. (Dordrecht: Kluwer), p.369
 Thompson, C. & Duncan, R.C. 1996, *ApJ*, 473, 322
 Tiengo, A., Goehler, E., Staubert, R., & Mereghetti, S. 2002, *A&A*, 383, 182
 Treves, A., Turolla, R., Zane, S., & Colpi, M. 2000, *PASP*, 112, 297
 Tsai, W.Y. & Erber, T. 1975, *Phys. Rev. D*, 12, 1132
 Zane, S., Turolla, R., Stella, L., & Treves, A. 2001, *ApJ*, 560, 384
 Zavlin, V.E. & Pavlov, G.G. 2002, in *Proc. 270 WE-Heraeus Seminar on Neutron Stars, Pulsars, and Supernova Remnants*, eds. Becker, W., Lesch, H., & Trümper, J., (MPE Rep. 278; Garching: MPI), p.263